JOURNAL OF MATERIALS SCIENCE 6 (1971) 1143–1150

The Morphology and Stability of Precipitates in Internally Oxidised Silicon-bearing Nickel and Cobalt Alloys

P. J. NOLAN, P. J. GRUNDY
Department of Pure and Applied Physics, University of Salford, Salford, Lancashire, UK

The results of an experimental investigation into the morphology of silica precipitates in internally oxidised silicon-bearing nickel and cobalt alloys are compared with the predictions of theories that concern the growth of spheroidal and extended precipitates and dendritic phases. Some degree of agreement is obtained between theory and experiment and a fairly detailed dependence of morphology on oxidation conditions and diffusion and concentration factors is outlined. Some observations on the stability of internal oxide precipitates are discussed and some conclusions, which are believed, in the main, to be general and applicable to any internally oxidised system, are made as to the dependence of morphology on the conditions of experiment.

1. Introduction

There have been many investigations of the internal oxidation process in dilute alloys. These studies have, in the main, been carried out with the aim of producing oxide dispersion-strengthened materials. Alloying elements such as silicon, aluminium, chromium, and thorium (all forming a refractory oxide) have been oxidised in silver [1], copper [2], nickel [3, 4] and other fairly noble matrices. Of particular relevance to the mechanical (and sometimes magnetic [4]) properties of the oxidised alloys, are the size distributions and states of dispersion of the oxide precipitates. In most strengthened systems, the precipitates are fairly small, typically $\sim < 0.1$ μm, and have simple morphologies, i.e. in the form of spheres, platelets or needles. It has been found that in some situations, internally oxidised silicon-bearing nickel [3] and cobalt alloys contain large silica precipitates which exhibit extremely complicated morphologies. The purpose of this paper is to describe these morphologies and to relate the formation of these structures to internal oxidation and growth conditions. Comparisons are made with results obtained on other internally oxidised alloys, in particular, other silicon-bearing alloys, and some general conclusions are given regarding the oxide morphologies in any internally oxidised system.

2. Experimental Procedure

The systems investigated were Ni-Si, Ni-Al and Co-Si alloys of varying Si and Al concentrations (< 2 wt % in all cases). These were prepared by arc melting under an argon atmosphere and were homogenised at 1200°C under an argon-hydrogen mixture. Rod-shaped pieces ($5 \times 2 \times 2$ mm) were spark cut from the ingots and internally oxidised in "Rhines packs" over a wide range of temperatures. After oxidation, the specimens were sectioned and mechanically and electrochemically polished to leave the inert oxide precipitates standing proud of the surface. The polished sections were vacuum coated with a thin layer ($\sim$ 200Å) of Au-Pd alloy to provide a conducting surface for the oxide precipitates and examined in a Cambridge "Stereoscan" scanning electron microscope.

3. Some Theoretical Considerations and Observed Morphologies

3.1. General Ideas

The factors governing the kinetics of internal oxidation are well known [5]. The phenomenon occurs in a dilute alloy if the following conditions are satisfied, (*a*) the oxygen pressure at the surface of the alloy is kept at the dissociation pressure of the solvent oxide at a particular temperature (this situation is assured if a Rhines pack [6] is used), (*b*) the free energy of formation

of the solute oxide, SO_ν, must be smaller (i.e. more negative) than that of the solvent oxide and (*c*) the diffusion coefficient of oxygen in the solvent, D_O, must be greater than the coefficient for the solvent, D_S, at a particular temperature. When these conditions hold, oxygen, at or less than the solubility limit, diffuses into the alloy and reacts with the solute to form molecules of the oxide SO_ν. Fig. 1 illustrates schematically the concentration profiles of oxygen and solute and the positions of the reaction front at a depth X and time t of oxidation.

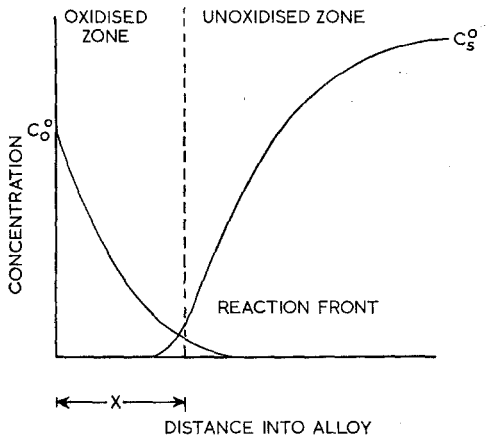

Figure 1 Ideal distribution of dissolved oxygen and solute atoms during the internal oxidation process.

Immediately behind the reaction front, which is defined as the plane in the alloy perpendicular to the oxygen flux at which the concentration of oxygen C_O is effectively zero, the SO_ν molecules exist in a supersaturated state and random nucleation of SO_ν occurs. Further growth of these particles occurs only if their radius r is greater than a critical size r_c given by basic nucleation theory, e.g. [7]. A nucleated particle has a sphere of influence in the alloy in which the concentration of reactants is reduced. This causes a local dissociation of SO_ν molecules and independent diffusion of S and O atoms to the particle surface where they subsequently re-associate. A result of this process is the setting up of concentration gradients for both O and S around a growing particle. This is the coagulation process.

3.2. Observed Morphologies

Some observations of internal oxidation in Ni-Si alloys have been reported [3, 8]. Some of the results shown by [3] were obtained by scanning electron microscopy (SEM). The striking feature of these observations is the variation of morphology of the silica precipitates with temperature of oxidation, depth below the alloy surface and silicon content. This variation is extreme and far more noticeable than in copper-based alloys [2]. Oxidation of Co-Si alloys also produced this extreme range of morphologies.

In general, all internally oxidised systems show a coarsening of the oxide dispersion with depth of oxidation [2]. Fig. 2*a* illustrates the morphology change from a spheroidal shape near the surface to a filamentary growth in the interior of the specimen. With lower silicon content alloys, cross-shaped particles, fig. 2b, or dendrites, fig. 2c, are produced. The simpler forms of precipitation generally occur nearer the alloy surface and/or furthest away from the oxidation front. Other workers [2] have noted the same departures from spheroidicity for silica particles in copper alloys, but have not made a detailed study of this. There is no doubt that SEM ameliorates previous experimental difficulties. In the following subsection, it is intended to relate morphology to determining factors such as alloy concentration, rate of oxidation and stability of the precipitates.

3.3. Conditions for Certain Morphologies

A stable spherical particle growing by the coagulation process in an isotropic concentration field, should retain its shape and enlarge until the supply of SO_ν is exhausted. However, it is possible to envisage a situation during internal oxidation where anisotropic fields occur, indeed it can be said that this is the general case in internal oxidation. It is possible for the internal oxidation front to travel at such a velocity through the specimen that the rate of growth of a precipitate is of the same order as the rate of internal oxidation. A particular nucleus, near the reaction zone, will grow as a sphere exhausting all the SO_ν from one side but will continue to draw more material from the direction of the front. In this situation the precipitate will lose its spherical shape and extend towards the front. Retention of spheroidicity by the precipitate through volume or surface diffusion of SO_ν molecules is slow relative to the growth process. The proposed conditions necessary for the loss of spheroidicity and the production of filamentary growths of SO_ν are:

(i) The oxidation front must move slowly so that

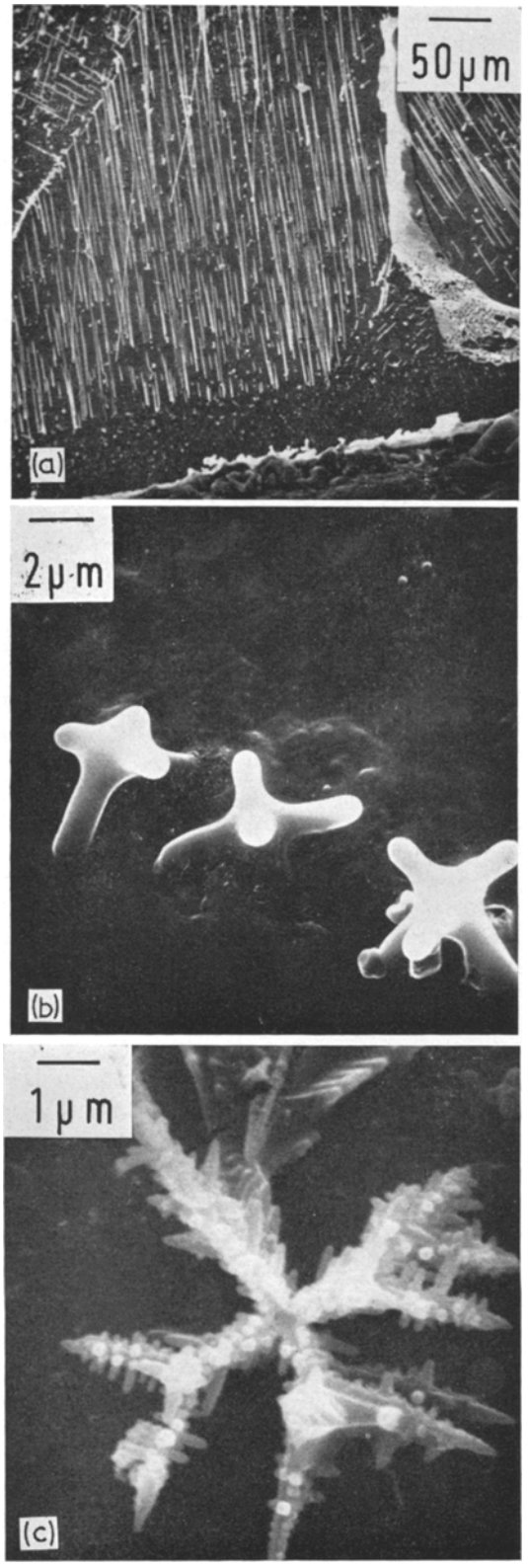

Figure 2 Variation of silica morphologies. (a) illustrates the change from spherical to filamentary growth with increase of depth in internally oxidised Ni-0.5 wt% Si. (b) cross-shaped precipitates and (c) dendrites in Co-0.08 wt% Si.

enough time exists for sufficient material to be provided to the extending precipitates ensuring that no nucleation centre forms between any one filament and the front. (This condition involves a particular relationship between the rate of oxidation and the rate of growth of the filament. If this relationship is violated in certain conditions, the filamentary growth is curtailed.)
(ii) The initial content of silicon is sufficient to provide the necessary growth rate.

The coagulation of spherical oxide precipitates has been quantitatively analysed by Serebryakov [9] who has derived an expression for the growth rate of an oxide which, for our experimental conditions, can be written,

$$\frac{dr}{dt} = \frac{D_s V k_\infty}{r(C_o)^2}\left[\left(\frac{k_o - k_\infty}{k_\infty}\right) - \frac{2\sigma V}{rkT}\right] \quad (1)$$

where k_∞ and k_o are equilibrium constants for the reaction $S + \nu O = SO_\nu$ at the surface of and at a distance from the particle respectively, V is the molar volume of SO_ν, σ is the surface energy of the interface and D_s is the diffusion coefficient of solute in the matrix. For the reaction $Si + 2O = SiO_2$, k_∞ is very small and can be neglected compared with k_o. Writing $k_o = (C_o)^2 C_s$ and neglecting terms in k_∞, equation 1 becomes,

$$\frac{dr}{dt} = \frac{D_s V C_s}{r} \quad (2)$$

where C_o and C_s are the concentrations of oxygen and silicon in the matrix.

In the case of the growth of a filament, the morphology of the precipitate naturally departs from spherical. However, for analytical purposes, the following assumptions will be made: (i) that the end of the filament extending in the direction of the oxidation front retains a hemispherical shape and keeps a constant radius of curvature, (ii) that the filament extends at the same rate as that of the motion of the oxidation front through the alloy. It follows from these assumptions that the end of the filament will grow in a constant environment and the steady state equation 2 can be used to express the rate of growth of this hemisphere. Thus the rate of lengthening of a filament is expressed as

$$\frac{dL}{dt} = \frac{D_S V C_S}{\rho} \quad (3)$$

where L is the length of the filament, ρ is the constant radius of curvature of the hemispherical end, and C_S is the initial content of silicon.

The filament will only grow if it can lengthen at a rate faster than or equal to that of the motion of the oxidation front. Thus, a condition of filamentary growth can be written

$$\frac{dL}{dt} \cos\theta \geqslant \frac{dX}{dt} \quad (4)$$

where θ is the angle between the direction of growth of the filament and the direction of motion of the oxidation front. Using the expression derived by Rhines [10] for the rate of internal oxidation, the following condition for filamentary growth is obtained.

$$X \geqslant \frac{\rho \sec\theta}{D_S V C_S} \cdot \frac{S}{M} \cdot \frac{C_O D_O - 0.84 \frac{O}{S} C_S D_S}{\frac{O}{S} C_S + \frac{C_O}{3}} \quad (5)$$

where O/S is in our case the ratio of the molecular weights of oxygen and silicon in the silica precipitate and S/M is that of silicon to the matrix element.

The conditions for filamentary growth are therefore only fulfilled after the oxidation front has penetrated to a distance X_F given by the equality in equation 5. In any one specimen, X_F is dependent on the temperature of oxidation (because C_O, D_O and D_S are functions of temperature), the original amount of silicon present in the alloy before oxidation, the angle at which the filament grows, and the thickness of the filament. Fig. 3 is a comparison between values of X_F calculated for various temperatures from equation 5 and experimental observations of X_F in internally oxidised Ni-0.5 wt % Si alloys. The theoretical results are computed using previous values of C_O [11], D_O [12] and D_S [13] with θ taken as zero and ρ as 0.5 μm. The value of X_F is observed to vary slightly within each specimen. This is because the value of θ cannot be calculated accurately from scanning electron micrographs. Thus only regions where filaments appear to grow approximately perpendicular to the surface of the specimen, are chosen for measurements. Errors occur in the high temperature values because of the instability of the filaments which will be discussed in a later section.

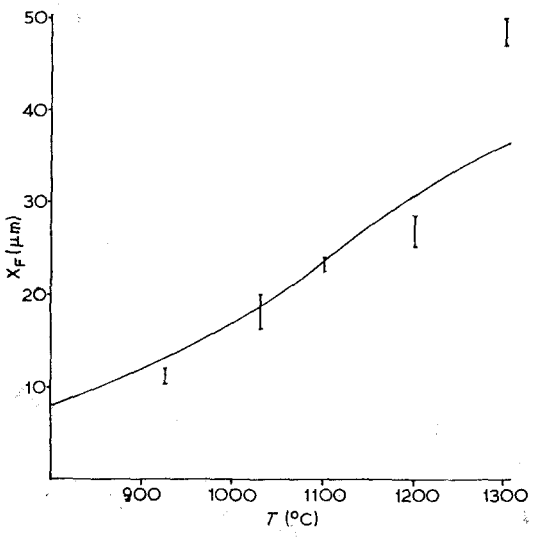

Figure 3 Comparison of theoretical and experimental values for the variation of X_F, the depth at which filamentary growth commences, with the temperature T.

The consistency between the calculated and observed values of X_F suggests that the proposed mechanism for filamentary growth is reasonable. It should also be noted that if similar theoretical values for X_F are calculated for Cu – $<$ 1 wt % Si, it is forecast that large values of X_F are needed before the commencement of filamentary growth. It is therefore not surprising that filaments have not been observed in dilute Cu-Si alloys [2]. In Ni-0.05 wt % Si, $X_F \sim 1$ mm at 1000° C and no filaments are observed [3].

It is interesting to observe the morphology of precipitates found in oxidised alloys of such a low silica content that, according to equation 5, filaments are unlikely to be seen. Fig. 4 illustrates the large variety of shapes that have been observed. The forms of the dendrites, fig. 4a, resemble those seen during the initial stages of crystal growth of metals from liquid melts. Chalmers [14] indicates that the empirical conditions for dendritic growth during solidification are: (i) the melt is subjected to only a low supercooling, and (ii) the solidifying material is crystalline. These should be compared to the present observations that: (i) dendritic growths occur during internal oxidation when the original silicon content is low (so that on oxidation, the nucleated silica molecules experience a relatively low supersaturation), (ii) some evidence has been reported [8, 15] that the precipitated silica is

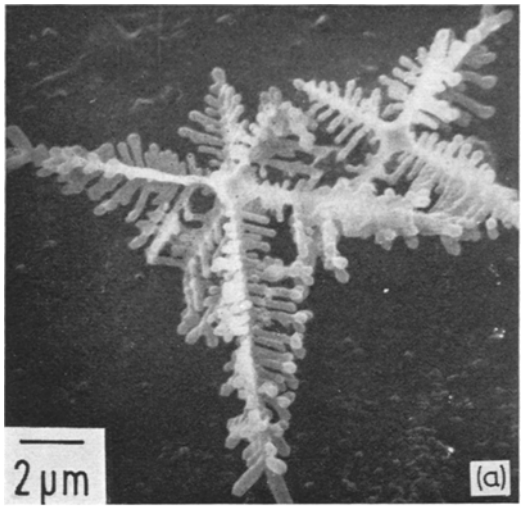

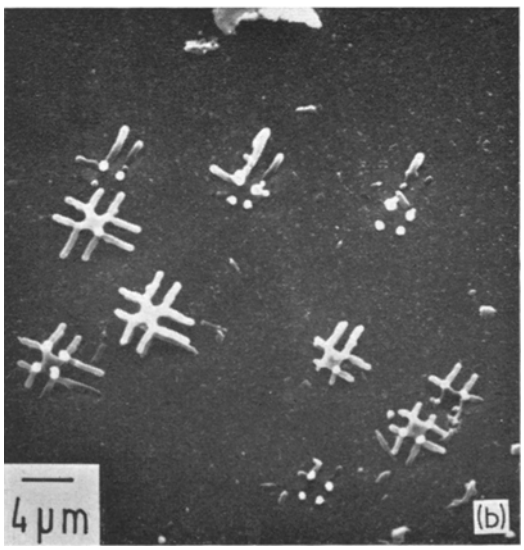

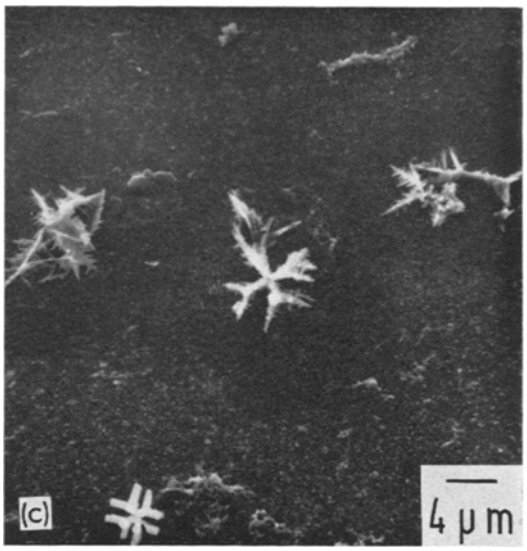

Figure 4 Silica precipitates in internally oxidised Co-0.08 wt% Si alloys. (a) dendritic growths closely resembling those seen during solidification from liquid melts. (b) cross-shaped structures assumed to be the result of breakdown in the dendritic form and are observed to exist in the same regions as dendrites. (c).

crystalline (this is discussed more fully in the next section). Both solidification and coagulation are diffusion controlled processes and it seems reasonable to assume that the growth mechanism of dendrites in very low silicon content alloys is similar to that of crystal solidification from a slightly supercooled liquid melt [16].

Fig. 4b illustrates another form of silica precipitate. These can exist in the alloys containing dendrites and are sometimes seen in the same areas (fig. 4c). However, these cross-shaped structures appear nearer the surface of a specimen than the dendrites. Dendrites tend to be confined to the regions near the oxidation front and evidence suggests that they are not stable structures but break down into cross-shaped or spherical particles after a short period of extended heating. (Stability will be discussed more fully in section 5.)

4. Dependence of Morphology on the Coherence of Precipitates

The extreme variations in the morphologies of observed precipitates with (i) silicon content, (ii) temperature of oxidation, and (iii) depth inside any particular specimen, seem to suggest that coherency between the oxide precipitates and the surrounding matrix is not a controlling factor in deciding the shape of the precipitate. However, a striking feature of both filaments and dendrites is the manner in which they are aligned parallel with each other in any one grain of the metal, fig. 5a. This indicates that at some early stage in the growth of the silica precipitates, there exists a coherency between the freshly nucleated particles and the surrounding matrix, which aligns the precipitates in the orientation of least misfit of the two lattices, and controls the early growth by restricting elongations to these directions of least misfit. Transmission electron microscopy on Ni-Si alloys [3] has shown that the directions of

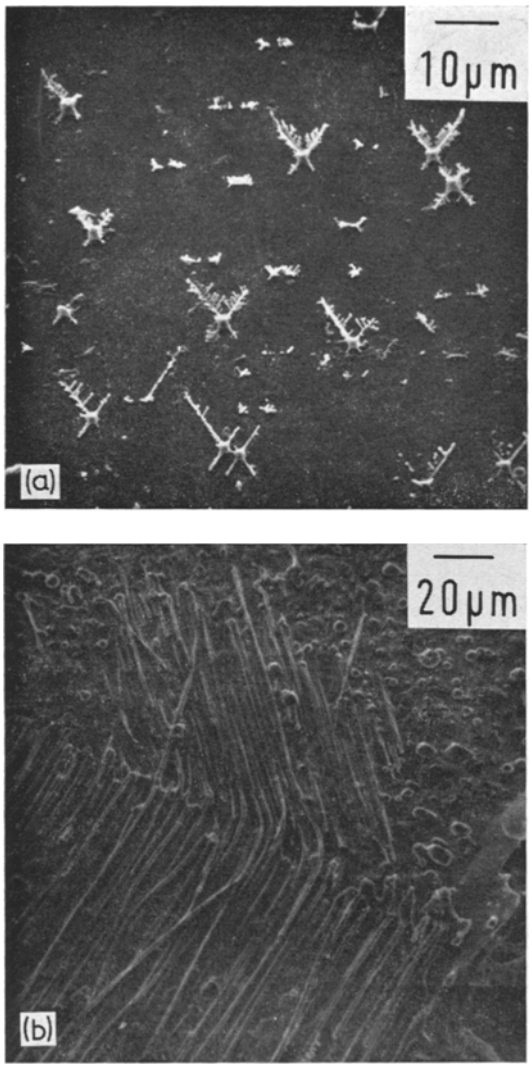

Figure 5 Effects of coherency on orientation of silica precipitates. These are illustrated by (a) the alignment of dendrites and (b) the bending of filaments when growing across a grain boundary.

elongation of silica precipitates are the ⟨100⟩ directions of the nickel matrix. All dendrites and side-growths on filaments display orthogonal growth directions. As stated above, it seems unlikely that coherency can control the final shape of the oxide and thus coherency must be lost when the particle reaches a certain size. Coherency is therefore only responsible for the direction of elongation of the nucleated sphere but the final shape is governed, as described in the previous section, by diffusion processes.

The possibility of coherency in the early stages of growth of the silica precipitates is, of course, closely linked to the structure of the silica. A recent X-ray investigation [8] has identified the silica as tridymite and some present electron diffraction results have indicated that extracted silica films and filaments can be partly crystalline in the form of crystobalite. However, most previous electron diffraction investigations [17, 18] and the present results suggest that the silica is completely or almost completely amorphous with, possibly, a small amount of crystalline phase present. If the front tip of a filament is small enough to retain coherency, it would seem that for amorphous silica the tip would be of the same order of size as a silica molecule and shaped in the form of a conic of large eccentricity. For crystalline silica, either as a crystalline precipitate or as a "core" in an otherwise amorphous filament, coherency would be lost at very small sizes. The electron diffraction evidence is proof of a very early transformation of the silica to an amorphous structure, and the suggestion that coherency is retained at small sizes either by an amorphous tip or crystalline "core", can only be conjecture at this stage of the work but it is certainly a possible reason for the observed orientation relationship of precipitates in the matrix and the change of direction of filaments on crossing a grain boundary, illustrated in fig. 5b.

5. Stability of Precipitates

The silica precipitates are found to be unstable and extended heat treatment of the internally oxidised alloy results in the spheroidisation of cylindrical filaments, fig. 6a. Breakdown begins immediately the filament is formed and thus occurs even as the internal oxidation process continues. This breakdown mechanism is believed to be a surface energy effect and therefore starts at the surface end of the filament which is, of course, the section formed first. Fig. 6b illustrates the early stages of the necking and spheroidising process. It is observed, fig. 6c, that cross-shaped silica particles are also unstable and break down leaving spheres still arranged in the original cross-shape. As mentioned in section 3.3, the dendrites are only observed near the oxidation front and instability results in the breakdown of dendrites to form cross-shapes before becoming spherical. Spheroidisation of alumina platelets has also been observed after the annealing of Ni-Al alloys, fig. 6d.

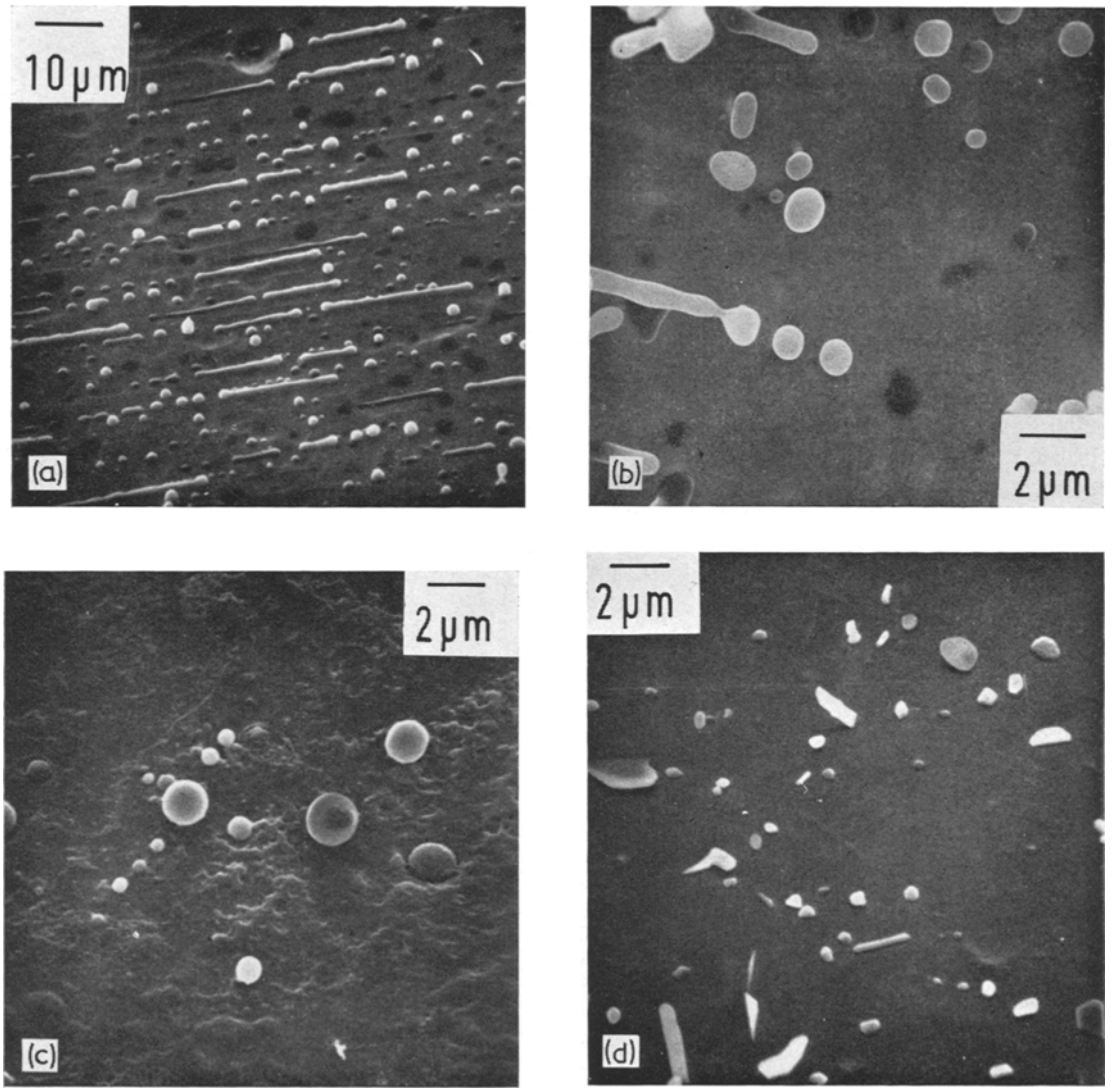

Figure 6 Instability of Oxide precipitates. (a) spheroidisation of filaments in internally oxidised Ni-1.5 wt% Si which was subjected to further heat treatment. (b) the necking process. (c) the breakdown of cross-shaped precipitates in annealed Co-0.08 wt% Si and (d) the spheroidising of alumina platelets in an annealed Ni-Al alloy.

6. Conclusion

The precipitate morphology in internally oxidised silicon-nickel and silicon-cobalt has been investigated as a function of oxidising temperature, concentration of solute and depth in the alloy. The morphologies observed, as clearly revealed by scanning electron microscopy, are often extreme and atypical of the internal oxidation systems usually investigated. A study of these morphologies has given an insight into the factors controlling the shape, and to some extent, size of internal oxide precipitates.

In the systems investigated it is concluded that coherency during very early stages of growth, or some other property, governs the orientation of non-spherical precipitates within the matrix. The relationship between orientations in different grains and across grain boundaries is strong experimental evidence for this control. However, the final shape is governed by diffusion

processes. Ample support for this conclusion is given by the successful explanation of filamentary growth by the invoking of anisotropic concentration fields in the region of the oxidation front. Under the assumption that a filamentary growth is stable over a short period of time, its presence in certain situations has been predicted. Extended oxide precipitates are expected in any internally oxidised system which contains sufficient amount of solute; the slower the rate of oxidation the sooner extended growth sets in.

The striking dendritic growths, observed at low solute concentrations, are suggestive of structures obtained in the solidification of supercooled liquid melts. It also is worth noting that Tiller and Mrdjenovich [19] have observed a change from lamellar to globular morphology with an increase of freezing rate during eutectic solidification. In this paper we have reported a change from spherical to filamentary growth with decrease of oxidation rate. These phenomena indicate that growth mechanisms during internal oxidation by diffusion of material in a supersaturated solid solution are analogous to the crystallisation and eutectic growth processes in supercooled liquid melts. Finally, observations of oxide structures which have undergone extended heat treatments, show that over long periods, surface energy effects tend to spheroidise the complex oxide precipitates.

Acknowledgements

The authors would like to thank Miss E. Burgess for assistance with the microscopy and acknowledge the EOOAR US Air Force for a maintenance grant (P.J.N.) through Grant EOOAR-68-005 and the SRC for a research grant.

References

1. E. GREGORY and G. C. SMITH, *J. Inst. Metals* **85** (1956-7) 81.
2. P. BOLSAITIS and M. KAHLWEIT, *Acta. Met.* **15** (1967) 765.
3. R. BARLOW, P. J. GRUNDY, and B. JOHNSON, *J. Mater. Sci.* **4** (1969) 359.
4. R. BARLOW and P. J. GRUNDY, *ibid* **5** (1970) 1005.
5. C. WAGNER, *Z. Elektrochem.* **63** (1959) 772.
6 F. N. RHINES, *Trans. AIME* **37** (1940) 246.
7. R. BECKER and W. DÖRING, *Ann. Phys.* **24** (1935) 719.
8. S. GOTO, K. NOMAKI, and S. KODA, *J. Japan Inst. Met.* **31** (1967) 600.
9. A. V. SEREBRYAKOV, *Soviet Phys. Solid State* **11** (1969) 778.
10. F. N. RHINES, W. A. JOHNSON, and W. A. ANDERSON, *Trans. AIME* (1941) Tech. Publ. No. 1368.
11. C. J. SMITHELLS, "Metals Ref. Book" (Butterworths, London, 1967) p. 631.
12. R. BARLOW and P. J. GRUNDY, *J. Mater. Sci.* **4** (1969) 797.
13. R. A. SWALIN, A. MARTIN, and R. OLSON, *J. Metals Trans. AIME* **207** (1957) 936.
14. B. CHALMERS, "Principles of Solidification" (Wileys, USA, 1964).
15. O. PRESTON and N. J. GRANT, *Trans. AIME* **221** (1961) 164.
16. G. F. BOLLING and W. A. TILLER, *J. Appl. Phys.* **32** (1961) 2587.
17. M. F. ASHBY and G. C. SMITH, *J. Inst. Metals* **91** (1962-3) 182.
18. S. L. CUNDY and P. J. GRUNDY, *Phil. Mag.* **14** (1966) 1233.
19. W. A. TILLER and R. MRDJENOVICH, *J. Appl. Phys.* **34** (1963) 3639.

Received 11 May and accepted 18 June 1971.